IJECBE (2026), **4**, **1**, 85–108
Received (6 January 2026) / Revised (10 March 2026)
Accepted (29 April 2026) / Published (30 March 2026)
https://doi.org/10.62146/ijecbe.v4i1.213
https://ijecbe.ui.ac.id
ISSN 3026-5258

International Journal of Electrical, Computer and Biomedical Engineering

RESEARCH ARTICLE

Design and Experimental Validation of an SDR-Based Private LTE Network for Flood Monitoring

Bambang Candra Wibawa* and Gunawan Wibisono

Department of Electrical Engineering, Faculty of Engineering, Universitas Indonesia, Depok, Indonesia
*Corresponding author. Email: bambang.candra@ui.ac.id

Abstract

The widespread impact of hydrometeorological disasters, such as floods, necessitated a reliable and rapidly deployable communication infrastructure to support real-time monitoring and early warning systems. During such events, conventional public cellular networks frequently collapsed, hindering critical information exchange. To address this vulnerability, the study presented the design and performance validation of a private LTE network based on softwaredefined radio SDR USRP B210 and open-source software, intended as a resilient backbone for an IoT-based flood monitoring system. The system was tested to assess its signal quality and user experience metrics across varying radial distances. Signal analysis confirmed severe channel degradation, with the SINR dropping from the "Excellent" category at 3 m to the "Fair" and "Poor" category at 9 m. This SINR decline directly caused the downlink throughput to fall drastically from 27 Mbps to a low of 2.8 Mbps and significantly inflated the maximum latency to 87 ms due to frequent HARQ retransmissions. A link budget analysis confirms that the limited communication range is primarily constrained by the low transmission power of the USRP B210 without external RF amplification. Despite these constraints, the network supported lowbandwidth IoT RSRP logging for modem consistency verification and sustained high-demand data services. The results validate the feasibility of SDR-based private LTE as a resilient communication platform for flood monitoring applications while clearly identifying system enhancements required for field deployment.

Keywords: 4G LTE, USRP B210, IoT, Flood Monitoring, Early Warning System

1. Introduction

Floods are one of the most widespread hydrometeorological disasters occurring in many parts of the world, including tropical regions such as Indonesia. According to a report released by the Central Statistics Agency (BPS) in 2024, at least 1,091 flood incidents occurred across various regions in Indonesia [1]. This disaster is generally caused by a combination of complex factors, such as climate change, environmental degradation, land use conversion, and poor spatial and environmental management, which are the primary causes of these flood disasters. Floods not only disrupt social and economic activities but also significantly impact physical infrastructure and public communication networks. Consequently, the economic impacts are widespread and substantially devastating [2]. In this context, the existence of a reliable communication infrastructure is becoming increasingly important, especially in supporting rapid response operations or disaster response missions. Along with the rapid development of communication technology, cellular communication systems have become an essential infrastructure for ensuring the smooth running of various aspects of daily life in today's modern era. The latest generation of cellular technology, such as 4G LTE, offers higher speeds, greater user capacity, and lower latency than its predecessors [3]. Among the many advantages offered by the 4G LTE network, this technology opens countless opportunities for integration across many sectors, including commerce, education, entertainment, and healthcare [4]. Furthermore, this technology plays a crucial role in environmental monitoring, early warning systems, and post-disaster relief operations [5].

In parallel with the digital transformation that has also reached the disaster management sector, IoT-based solutions are increasingly being adopted to improve the effectiveness of flood monitoring systems in supporting mitigation efforts. Sensors are installed at key locations to measure parameters such as water levels, rainfall intensity, and water flow. The data from these sensors are transmitted in real-time to a central server for analysis, serving as the basis for decision-making or activating EWS. Dui et al. [6] proposed an IoT-based framework to help sponge cities become more resilient to flooding. This approach combines surface rainwater management and drainage infrastructure with a layered system that monitors hydrological conditions in real time. Cities can respond to flooding more quickly and efficiently, especially during the increasingly unpredictable challenges of climate change. Zakaria et al. [7] developed a smart sensor unit for power-efficient and scalable LoRaWAN-based flood monitoring for rainfall catchment areas in Malaysia. The system can send real-time water level data to multiple cloud platforms, providing risk-based early warnings. The system is designed to be easily accessible to the public via dashboards and mobile applications. It also demonstrates good communication performance in real-world scenarios. Prakash et al. [8] developed an IoT-based flash flood monitoring and prediction system for mountainous regions, such as Uttarakhand, India. This system is capable of accurately classifying flood danger levels in real time while also providing early warnings via an Android application by combining inexpensive sensors and LSTM. Performance evaluation was conducted using the RMSE, precision, recall, and F1-score metrics.

However, most flood monitoring systems implemented to date still rely on public communication infrastructure, commercial cellular networks, Wi-Fi, and fiber optic cables. These networks often experience disruptions when disasters occur, and in the worst-case scenario, they can collapse completely due to physical damage to infrastructure, power outages, or overcapacity [9]. Consequently, this hinders the distribution of emergency information to authorities and the public. This reliance on conventional communication systems is a weakness that could eventually collapse, especially in emergency situations where the speed and reliability of information exchange are critical. Ultimately, the distribution of critical information, such as early warnings, flood condition updates, and evacuation instructions, is hindered, which can worsen the negative impacts of disasters on human safety and material losses [10], [11]. Makino et al. [12] evaluated the effectiveness of private LTE networks in multi-story buildings, particularly in terms of data speed (throughput), latency (delay), and signal quality (RSRP). Using an AGV robot to automatically collect data while moving across various floors. The results revealed that communication scheduling requests significantly affected data delay, especially for uplink communications. This study highlights that private LTE could be a more stable alternative to Wi-Fi in indoor environments such as factories and office buildings. Gomez et al. [13] proposed an LTE network design that can continue to function even if the main infrastructure is damaged by a disaster. Each node (network device) can stand alone and connect to each other via a mesh network. This allows emergency response teams to continue communicating even when conventional networks are down. This approach is suitable for use in disaster-prone areas or in emergencies such as earthquakes and floods. Mishra N et al. [14] demonstrated how the srsRAN stack can be expanded by wirelessly connecting the base station and core. This means that LTE networks can be built in a distributed, wireless form that is suitable for disaster areas or large regions. The results show that srsRAN is sufficiently flexible to be applied in various field conditions that require quick installation and minimal infrastructure.

In such a scenario, the adoption of a private LTE network system is a highly promising solution. This is because it enables the system to operate independently of the public cellular communications infrastructure, which is often vulnerable to interruption during disasters. Furthermore, a private LTE network can be customized to suit the specific operational requirements on-site, including coverage area, number of users, and the prioritization of quality of service (QoS) [15], [16], [17]. This work presents a design for an LTE communication network system based on software-defined radio (SDR) USRP B210 in a tactical box. The main advantage of USRP is its ability to perform real-time digital signal processing with high speed and precision, and it can function as a transmitter and receiver in radio and cellular communication systems. USRP radio hardware has been widely used in the fields of research, mobile network protocol testing, education, and the development of wireless communication technologies such as long-term evolution (LTE) and 5G [18], [19]. This system is built by leveraging open-source software and combined as the backbone network of an IoT flood monitoring system. This system aims to establish resilience in cellular communication networks that can be rapidly deployed within minutes in disaster-prone and affected areas, where public communication infrastructure is often disrupted.

The negative impacts of disasters are expected to be effectively mitigated with this design, ensuring the continuity of real-time and sustained connectivity between the IoT-based flood monitoring system and the central server.

2. Methodology

This study is conducted using a quantitative systems engineering approach, using experimental and evaluative methods. The LTE architecture was configured with a fixed system bandwidth of 10 MHz, corresponding to 50 resource blocks. Bandwidth selection serves as a critical determinant for both the noise floor and achievable throughput. Although expanding the bandwidth enhances maximum throughput capacity, it concurrently elevates noise power. This trade-off can potentially degrade SINR in low-power transmission scenarios. Therefore, the bandwidth selected for this study deliberately exceeds the minimum requirements for flood monitoring IoT data. This design choice ensures that any observed throughput degradation is attributable to radio channel conditions rather than bandwidth constraints.

The telemetry payload used in this study was 85 bytes transmitted every 1 s, corresponding to a raw application-layer data rate of approximately 680 bps per device. The actual end-to-end traffic load is higher than this lower-bound value because HTTPS delivery introduces additional transport, network, and protocol overhead. Consequently, the configured LTE bandwidth of 10 MHz was intentionally much larger than the minimum telemetry requirement, allowing the observed performance degradation to be interpreted primarily as a radio-channel and link-budget effect rather than a bandwidth-limited application effect.

2.1 Link Budget Analysis

A link budget analysis based on the experimental system configuration was performed to account for the observed communication range and the accelerated degradation of signal quality. The SDR-based transmitter utilized in this testbed yields a lower effective radiated power (EIRP) than commercial LTE eNodeB platforms. This disparity stems primarily from the absence of a dedicated high-power RF amplification stage in the experimental setup. When factored alongside modest antenna gains and inherent insertion losses from RF cables, connectors, and front-end components, the resulting link margin is significantly restricted. Consequently, the received signal quality diminishes rapidly as separation distance and environmental attenuation increase, precipitating a sharp reduction in SINR and a corresponding decline in downlink throughput. The received signal power P_γ can be estimated using the standard link budget equation:

$$P_r = P_t + G_t + G_r - L_p - L_s \tag{1}$$

Where:

a) P_γ denotes the received power at the receiver [dBm].
b) P_t denotes the transmit power at the transmitter output [dBm].
c) G_t represents the transmit antenna gain [dBi].
d) G_γ represents the receive antenna gain [dBi].

e) L_p refers to the propagation path loss due to distance and channel conditions [dB].
f) L_s refers to the total system losses [dB].

All experimental measurements in this study were conducted in an indoor environment, which represents a conservative propagation condition due to rich multipath, penetration losses from walls and furniture, and strong signal reflections. These effects can reduce SINR and spectral efficiency over short distances, and the impact becomes more pronounced when the transmitter operates without an external RF front-end and with limited effective radiated power. To maintain a reproducible analytical baseline, the framework adopts the free-space path loss (FSPL) model in Equation 4 as a minimum-loss LOS reference. Using FSPL as a lower-bound path-loss baseline intentionally yields conservative estimates for the radiated-power terms: any additional indoor excess loss beyond FSPL would require a higher EIRP to achieve the same received power.

To provide a quantitative explanation of the observed short-range behavior and to support reproducibility, we report an effective lower-bound estimate of the transmitter's radiated power. When a calibrated conducted-power measurement at the RF port is not available, the effective equivalent isotropically radiated power (EIRP) can be conservatively inferred from the wideband received power and a minimum-loss propagation baseline. Accordingly, we estimate a lower bound of EIRP by combining the inferred RSSI with FSPL, as expressed:

$$EIRP_{LB}(dBm) \approx RSII(dBm) + FSPL(d,f)(dB) \tag{2}$$

Where:

a) $EIRP_{LB}$ denotes the lower-bound estimate of the effective isotropically radiated power of the transmitter under the experimental configuration [dBm].
b) $RSII$ denotes the received signal strength indicator, i.e., the wideband received power over the configured LTE bandwidth [dBm].
c) $FSPL(d,f)$ denotes the free-space path loss at separation distance d and carrier frequency f (minimum-loss LOS baseline) [dB].
d) d denotes the transmitter-receiver separation distance (expressed in km in the FSPL formula) [km].
e) f denotes the carrier frequency (expressed in MHz in the FSPL formula) [MHz].

After obtaining a conservative lower-bound estimate of the effective isotropically radiated power ($EIRP_{LB}$), we translate the radiated-power term into an equivalent effective conducted transmit power at the transmitter RF output. This step is necessary to relate the link-budget interpretation to reproducible hardware parameters and to explicitly quantify the transmitter side limitation under the baseline SDR configuration. The effective conducted transmit power lower bound is obtained by accounting for the transmit antenna gain and the TX chain losses, as expressed:

$$P_{tx,LB}(dBm) \approx EIRP_{LB}(dBm) - G_{tx}(dBi) + L_{tx}(dB) \tag{3}$$

Where:

a) $P_{tx,LB}$ denotes the effective conducted transmit power lower bound at the transmitter RF output [dBm].
b) $EIRP_{LB}$ denotes the lower-bound estimate of the effective isotropically radiated power [dBm].
c) G_{tx} represents the transmit antenna gain [dBi].
d) L_{tx} represents the total transmit-chain loss including cable and connector losses [dB].
e) The approximation reflects a conservative bound because $EIRP_{LB}$ is inferred using FSPL as a minimum-loss LOS baseline, while indoor excess losses (clutter/multipath) can be higher.

The FSPL term used in the following computations is defined in Section 2.2 and is treated as a minimum-loss LOS baseline. This choice yields a conservative lower-bound estimate for $EIRP_{LB}$ and $P_{tx,LB}$.

Table 1. Link-budget-based lower-bound estimate of effective radiated power and conducted transmit power under the baseline SDR configuration.

Distance (m)	RSRP (dBm)	RSSI (dBm)	FSPL (dB)	$EIRP_{LB}$(dBm)	$P_{tx,LB}$(dBm)
3	-92	-64,2	41,5	-22,7	-24,3
6	-100	-72,2	47,5	-24,7	-26,2
9	-105	-77,2	51,0	-26,2	-27,7

2.2 Indoor Test Environment and Outdoor Deployment Context

Performance validation was conducted within a controlled indoor laboratory environment to prioritize repeatability and safety during the initial prototyping phase. Indoor radio propagation typically introduces more pronounced multipath fading, scattering, and shadowing effects from structural elements and human activity than would be expected in outdoor riverbank or openarea deployments. Consequently, the SINR and throughput degradation observed indoors at relatively short distances serves as a conservative, worst-case performance indicator rather than an absolute limitation for outdoor coverage.

Beyond these environmental factors, the achievable communication range in this study is further constrained by the limited RF output capability of the SDR-based eNodeB when operated without an external RF front-end. Compared to commercial LTE eNodeB hardware, this configuration yields a lower effective radiated power and a reduced link margin, particularly under non-line-of-sight and multipath-rich conditions. Therefore, the rapid SINR degradation observed at extended indoor distances reflects the synergistic impact of severe indoor channel characteristics and the constrained link budget inherent in the current prototype design.

To bridge laboratory results to field practicability, an outdoor line-of-sight (LOS) reference path loss baseline can be approximated using the free-space path loss (FSPL) model:

$$PL_{FS}(dB) = 20log_{10}(d) + 20log_{10}(f) + 32.44 \tag{4}$$

Where:

a) d denotes the distance between the transmitter and the receiver (kilometers).
b) f denotes the signal frequency (MHz).
c) 32.44 denotes a constant used for unit conversion and adjustment for distance and frequency.

Under outdoor LOS conditions, where multipath and penetration losses are substantially mitigated, the same system configuration is expected to achieve improved SINR and more stable connectivity over longer distances. To contextualize the indoor measurements against the intended outdoor deployment scenario, we provide an outdoor Line-of-Sight (LOS) propagation reference using the free-space path loss (FSPL) model. Table 2 summarizes the FSPL values at representative field distances (100 m, 300 m, and 1 km) for the operating carrier frequency of 942.5 MHz, serving as a minimum-loss baseline for practicability assessment.

Table 2. FSPL-based outdoor LOS path loss reference for flood-monitoring deployment distances (942.5 MHz)

Distance	d_{km}	FSPL (dB) at 942.5 MHz
100 m	0.10	71,9
300 m	0.30	81,5
1 km	1	91,9

While FSPL provides a fundamental baseline for unobstructed LOS conditions, outdoor deployments require additional margins for terrain shadowing, vegetation-induced attenuation, antenna installation height, polarization mismatch, and time-varying fading. Hence, Table 2 should be treated as an idealized lower-bound reference, and robust field deployments should include fade margins and RF front-end enhancements to ensure reliable hectometric coverage.

2.3 Universal Software Defined Radio (USRP)

Software defined radio (SDR) is a radio communication technology that incorporates most of the functions of traditional radios, such as modulation, demodulation, filtering, and signal detection. Therefore, protocols can be configured and updated without changing the hardware, allowing SDR to enable the development and operation of highly flexible communication systems [20]. Figure 1 shows the SDR architecture comprising RF/IF blocks, digital front end, and baseband processing components.

Referring to Figure 1, the SDR architecture is divided into two parts. The first is the hardware, which includes the antenna, radio frequency (RF) front end, analog-to-digital converter (ADC), and digital-to-analog converter (DAC), and the software part that manages digital signal processing (DSP) run by a field-programmable gate array (FPGA). Among the various types of SDR devices available on the market, the

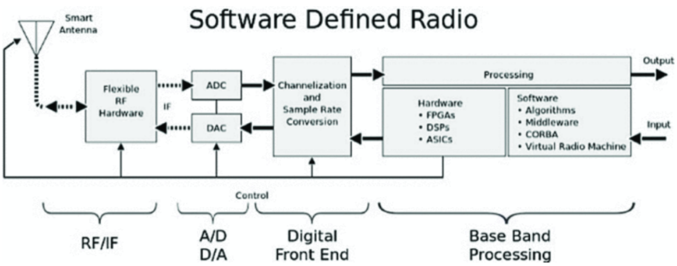

Figure 1. The system architecture of the SDR [21]

Figure 2. The USRP B210 used for the research

most popular device is the USRP B210 shows in Figure 2, which will be utilized in this research as an RF front-end device for LTE signal transceiver.

The Universal Software Radio Peripheral B210 is an SDR-based hardware device developed by Ettus Research. The USRP is designed to provide flexibility, as it can be configured according to user needs. The USRP has a frequency coverage of 70 MHz – 6 GHz with a bandwidth of up to 56 MHz, making it very supportive in the development of wireless communication systems through software-based analog and digital signal processing [22].

2.4 srsRAN

srsRAN is an open-source software platform (formerly known as srsLTE) developed by Software Radio Systems. Currently evolving into a more sophisticated solution, srsRAN is tailored to establish end-to-end 4G and 5G long-term evolution (LTE) cellular communication networks for network architecture, including Evolved Packet Core (EPC), evolved Node B (eNB), and user equipment (UE) [23]. As shown in Figure 3, the component-level diagram of the proposed portable private LTE system shows that the srsEPC and srsENB components are installed under the same system PC.

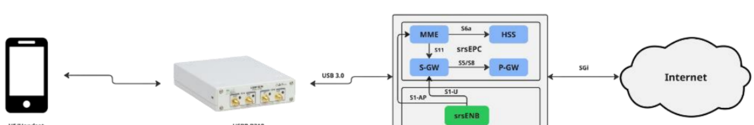

Figure 3. Component-level diagram of srsRAN with USRP B210 setup

With the existence of the srsRAN, it is made it possible for anyone to build their own or independent mobile networks that are technically functional in compliance with the 3rd Generation Partnership Project (3GPP) standards. The srsRAN is supported by the 3GPP standards release 10 to release 15 for LTE networks, and release 17 for 5G networks [24], [25].

2.5 System Model

2.5.1 Configuration of Portable LTE System

The private LTE communication system was executed through a systematic approach, prioritizing real-time signal processing stability and rapid field deployment capability within a compact platform. This methodology is detailed across four primary stages: platform configuration, core and radio network implementation, system integration, and performance validation. Figure 4 shows the comprehensive architecture of the proposed system, in which the srsRAN PC will be installed with EPC, eNB, and UHD (USRP Hardware Driver). This PC will be powered by a battery to increase the system's portability and allow the system to operate offgrid without any external power sources.

Figure 4. Comprehensive architecture of the portable LTE private system

The network's foundation was a dedicated computing server using Ubuntu Server 22.04 LTS. This operating system was selected primarily for its robust, low-latency kernel support and comprehensive native compatibility with the UHD (USRP Hardware Driver). Crucial hardware resources, specifically 16 GB of RAM and 512 GB SSD storage, were mandated to ensure efficient memory allocation for baseband signal processing and to mitigate I/O (Input/Output) bottlenecks, which are critical for maintaining the stability of the SDR application during highload operation.

The software stack was built on the srsRAN open-source suite. This package was leveraged to implement the full 3GPP LTE stack functionality on a single platform, integrating the EPC and RAN components. This choice was justified by the flexibility of srsRAN and its ability to realize a complete end-to-end network environment using software-defined parameters. The srsEPC component, which encompasses the Mobility Management Entity (MME), Home Subscriber Server (HSS), and Gateways (SGW/PGW), was rigorously configured. The user authentication data were provisioned onto the HSS database (user _ db.csv), which is central to network access. This process required setting precise security parameters, specifically the International Mobile Subscriber Identity (IMSI), the subscriber key (Ki), and the Derived Operator Code (OPC), which were strictly mirrored within the MME configuration for robust mutual authentication during user attachment. Furthermore, to facilitate data flow to client devices, IP forwarding was activated, and NAT rules were strategically implemented within the firewall's IP tables, ensuring efficient routing of user traffic between the internal network and the external data interface. The srsENB was configured to operate using the USRP B210 as the radio frontend, which was connected to the server via a USB 3.0 port to support the required high-speed data throughput. The system was parameterized for operation in LTE FDD Band 8 at a downlink center frequency of 942.50 MHz (EARFCN 3625). The selection of this lowerfrequency band was a deliberate technical decision justified by its superior propagation characteristics in remote and obstructed field environments, thus maximizing the overall coverage footprint [26], [27]. An appropriate LTE antenna was connected via SMA interfaces to enable over-the-air transmission. The entire private LTE components, including the computing unit, USRP B210, antenna interfaces, and battery pack, were encapsulated within a custom-built ruggedized platform (manpack), as shown in Figure 5.

Figure 5. Physical setup of the proposed private portable LTE system

This design solution was crucial for achieving operational independence and facilitating rapid deployment in emergency or remote scenarios, thereby eliminating reliance on existing public telecommunication networks, as shown in Figure 5. It also supports off-grid operation for up to 6 h using an internal 288 Wh battery, removing the need for external power. The network functionality was subsequently verified by inserting a customized user equipment User Equipment (UE) SIM card into a mobile phone and the LTE IoT modem.

The detailed hardware specifications and system parameters used in this implementation are summarized in Table 3, including the SDR configuration, antenna characteristics, and key RF settings. This table provides essential information to ensure experimental reproducibility and to support future system scaling for real-world deployment scenarios.

Therefore, a wider bandwidth can slightly reduce SINR for the same received signal power, while a narrower bandwidth improves robustness at the expense of peak data rate. This trade-off is important for low-bandwidth flood telemetry, where reliability is prioritized over maximum throughput.

Table 3. Key hardware specifications and system parameters of the experimental setup

Parameters	Details
SDR platform	USRP B210, 70 MHz-6 GHz
Base station software stack	srsRAN (srsEPC + srsENB) on a single host PC
Operating system	Ubuntu Server 22.04 LTS
Host computer resources	16 GB RAM, 512 GB SSD
Operating band and carrier	LTE FDD Band 8, DL center frequency 942.50 MHz (EARFCN 3625)
LTE channel bandwidth	10 MHz (50 PRBs)
Antenna type and gain	Omnidirectional SMA LTE antenna (∼2 dBi)
TX chain losses	Short SMA pigtail + connector loss (∼0.5 dB)
External RF front-end	None (no external PA/LNA used in baseline experiment)
Power supply	288 Wh battery pack
Internet/backhaul for external access	30 Mbps dedicated connection
Measurement plan	30 repeated measurements per distance (3 m, 6 m, 9 m)
Effective conducted TX power (lower-bound estimate), $P_{tx,LB}$	-26 dBm

2.5.2 Radio Measurement Metrics and Conversion

In this study, radio performance is quantified using UE/modem-reported metrics that are commonly used to characterize LTE downlink signal conditions and their impact on link reliability. Specifically, we report Reference Signal Received Power (RSRP) as the primary coverage indicator, and we infer the wideband received power (RSSI) to support power-path reasoning and link-budget interpretation under the configured LTE bandwidth. RSRP represents the average received power of LTE reference signals (pilots) and is less sensitive to instantaneous traffic load, making it suitable for comparing distance-dependent coverage under controlled conditions. Measurements were collected at each test distance for multiple runs to reduce random fluctuations caused by multipath and short-term fading.

To obtain an estimate of the wideband received power over the configured LTE carrier, RSSI is inferred from RSRP using the LTE resource-block relationship, expressed as:

$$RSSI(dBm) \approx RSRP(dBm) + 10log_{10}(12N_{PRB}) \tag{5}$$

Where:

a) RSRP denotes the reference signal received power reported by the UE/modem, representing the received power of LTE reference signals [dBm].
b) RSSI denotes the received signal strength indicator, i.e., the estimated wideband received power over the configured LTE bandwidth [dBm].
c) N_{PRB} denotes the number of physical resource blocks corresponding to the configured LTE bandwidth.

To connect UE-reported measurements with a power-path interpretation, the inferred wideband received power (RSSI) is used as an intermediate term in the subsequent link-budget analysis. In particular, RSSI is combined with a minimum-loss propagation baseline (FSPL) to obtain a conservative lower-bound estimate of the effective isotropically radiated power, $EIRP_{LB}$, and the corresponding effective conducted transmit power bound under the experimental configuration. This approach provides a traceable explanation of the short-range behavior observed in indoor tests and motivates the RF front-end enhancements required for field-scale deployments.

2.5.3 IoT Configuration

The core of the measurement system used a single-board computer (SBC) Raspberry Pi to function as the edge computing unit. This choice was strategically implemented because of its optimal balance of low power consumption and robust GPIO flexibility, which are essential for managing real-time sensor data acquisition and executing the Python-based control logic in a field environment. The successful deployment and operation of the proposed portable private LTE network can be evidenced by the real-time transmission of water level data from the IoT flood monitoring system to the Blynk server, as illustrated in Figure 6.

As illustrated in Figure 6, Blynk served as the backend-as-a-service (BaaS) platform, providing the necessary infrastructure for data visualization, archival, and remote monitoring of the water level indicators by end-users. The HC-SR04 ultrasonic sensor managed the distance measurement, specifically the water level, which leverages the time-of-flight principle to calculate the distance between the sensor and the water surface via reflected sound waves. Subsequently, this distance data is converted into an accurate water level reading. Furthermore, the system incorporates a buzzer as a critical local actuator designed to provide immediate, nonnetworked sound warnings when the water level reaches predefined minimum and maximum threshold values.

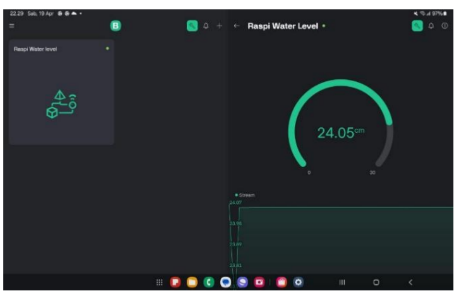

Figure 6. Real-time visualization of the water-level monitoring system using the Blynk IoT platform

3. Evaluation of Performance

Evaluation of Performance In evaluating the performance of the proposed portable private LTE network, the assessment deliberately focuses on three key radio performance metrics: RSRP, RSRQ, and SINR. This emphasis is necessary because these specific radio metrics play a crucial and indispensable role in maintaining the sustained data connectivity or quality of service (QoS) between the user equipment and the underlying communication infrastructure, as well as reflecting signal strength, quality, and link reliability, respectively [28], [29], [30].

A) RSRP

The RSRP is the average strength of a signal transmitted from a cell tower as it is received by a mobile device. A high RSRP indicates a strong signal and supports better services, such as stable connections and high speeds, whereas a low RSRP indicates a weak signal that can degrade service quality. The RSRP is expressed as follows:

$$RSRP = RSSI - 10xlog10(12xN) \tag{6}$$

Where:

a) N is number of Resource Blocks (RB) used on the channel.
b) *TheRSSI* represents the total received signal strength in one subframe, including the reference signal, interference, and noise.

Standardized measures are usually applied for critical parameters to evaluate signal quality in LTE networks. For RSRP:

Table 4. RSRP thresholds and the corresponding cell signal strength categories [31]

RSRP	Signal Strength
>-90 dBm	Excellent
- 90 to -105 dBm	Good
- 106 to -120 dBm	Fair
<-120 dBm	Poor

B) RSRQ

The RSRQ is a signal quality measure that considers interference and noise, reflecting how clean the received signal is. The RSRQ is expressed in decibels (dB). High RSRQ values reflect good network quality, and low RSRQ values reflect poor network quality, reflecting interference that could degrade service performance. The RSRQ is calculated from the RSRP and RSSI ratio, as defined by the equation:

$$RSRQ = \frac{NxRSRP}{RSSI} \tag{7}$$

Where:

a) N represents the number of used resource blocks.
b) *RSRP* represents the average of the received reference signal power.
c) *RSSI* for total received power, including signal, interference, and noise.

Table 5. RSRQ thresholds and associated signal quality levels in LTE/5G networks [31]

RSRQ	Signal Strength
>-9 dB	Excellent
- 9 to -12 dB	Good
<-13 dB	Fair to Poor

C) SINR

SINR indicates the desired signal-to-noise ratio in the network, which reflects the ability of the received signal to be processed by the device. SINR is in decibels (dB), and a high SINR implies good signal quality, whereas a low SINR implies interference that can reduce the quality of the connection. This can be explained by the following formula:

$$SINR = \frac{P_{signal}}{P_{interference} + P_{noise}} \tag{8}$$

Where:

a) P_{signal} is the average received signal power.
b) $P_{interference}$ is the average power of the interference from other cells or sources.
c) P_{noise} is the power of the random noise in the network.

Standardized measures are usually applied for critical parameters to evaluate signal quality in LTE networks. For SINR:

Table 6. SINR thresholds and the corresponding expected channel throughput [31]

SINR	Throughput
>10 dB	Excellent
6-10 dB	Good
0-5 dB	Fair
<0 dB	Poor

4. Results and Discussion

4.1 Performance Analysis of LTE Channel Quality and User Experience Metrics

Referring to the standardized thresholds in Table 4 and the empirical results presented in Figure 7, the RSRP values reveal a clear signal quality transition corresponding to path loss. At 3 m, the RSRP is predominantly in the "Excellent" category. Conversely, measurements at 6 and 9 m distinctly transition, with the majority falling in the "Good" category, though the lowest readings briefly touch the "Fair" range. This RSRP degradation occurs because of the accentuated impact of physical obstacles and electromagnetic wave phenomena during propagation. Signals cross numerous obstacles at farther distances, causing signal power to be depleted before reaching

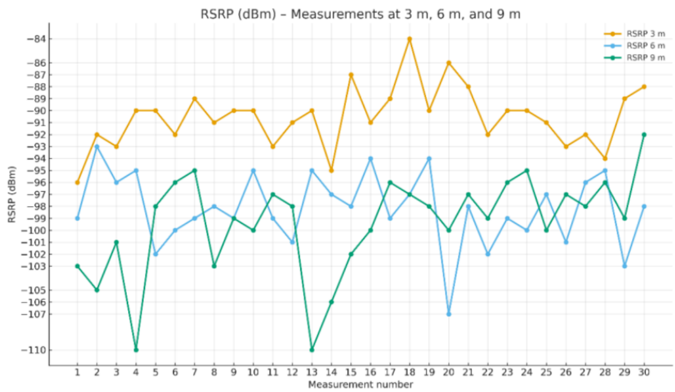

Figure 7. Measured RSRP values at distances of 3, 6, and 9 m

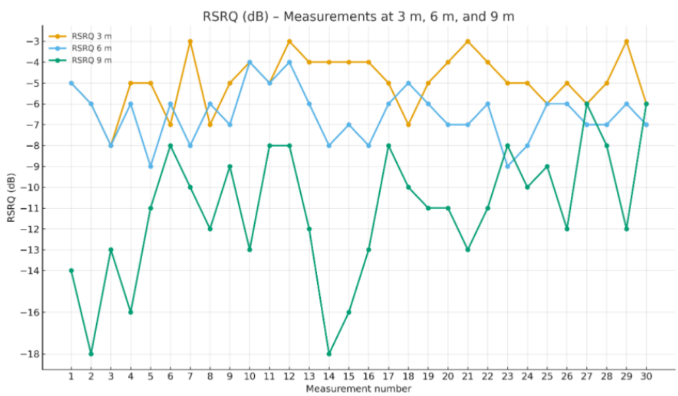

Figure 8. Measured RSRQ values at distances of 3, 6, and 9 m

the user's device. Multipath and fading effects may worsen this situation by creating dynamic fluctuations in the received signal [32].

The quality of the received signal, evaluated through RSRQ, is a key performance indicator that fundamentally quantifies the impact of both interference and noise relative to the useful signal power. Analysis of the RSRQ results presented in Figure 8 against Table 5 reveals a pronounced decline in the stability of signal quality. At 3 m, the RSRQ measurements are highly stable, remaining firmly in the "Excellent" category. At 6 m, the quality frequently touches the "Good" boundary. Crucially, the 9 m measurements exhibit extreme volatility. While the highest readings remain "Excellent," the frequent drops below the -13 dB threshold force a significant portion of the data into the "Fair to Poor" category. This volatility confirms that interference and multipath effects become dominant limitations at extended distances, resulting in an extremely low signal-to-noise ratio (SINR) and directly limiting achievable throughput due to higher error rates.

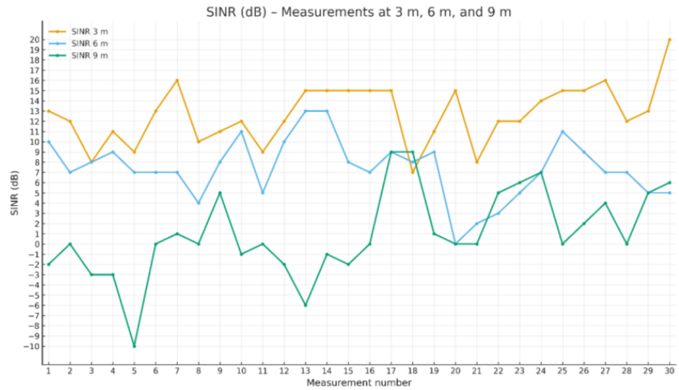

Figure 9. Measured SINR values at distances of 3, 6, and 9 m

Following the degradation noted in RSRQ, the SINR is the single most critical factor dictating the channel capacity. Analysis of the SINR results against the thresholds in Table 6 confirms a severe decline in the spectral efficiency potential (Figure 9). At 3 m, the SINR is consistently in the "Excellent" category. This condition facilitates the use of high-order Modulation and Coding Schemes (MCS), maximizing the bit rate. However, the quality rapidly deteriorates with distance. At 6 m, the SINR is predominantly found in the "Good" category, although it frequently drops into the "Fair" category. The most critical impact is observed at 9 m, where the data exhibit extreme volatility. The SINR consistently falls into the "Fair" and "Poor" categories, with minimum values reaching levels significantly below 0 dB. This sustained low SINR forces the eNodeB to select the least efficient MCS, thereby establishing the definitive bottleneck on Downlink Throughput, as shown in Figure 9.

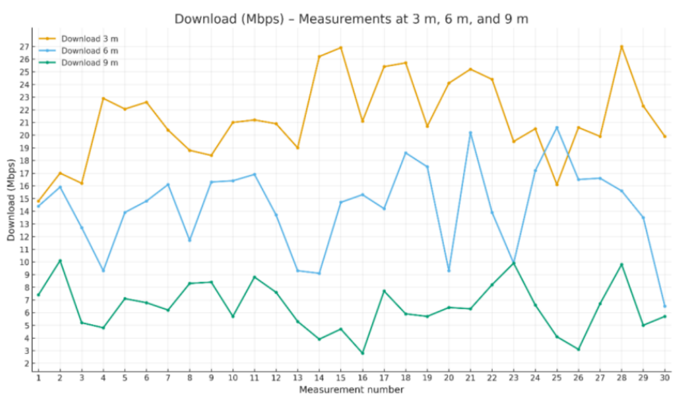

Figure 10. Measured download values at distances of 3, 6, and 9 m

The direct consequence of the sharp degradation in SINR is observed in the Downlink Throughput performance, as shown in Figure 10. This metric reflects the end-user experience and physical layer efficiency. At 3 m, the throughput is maximized, achieving speeds of up to 27 Mbps with minimal fluctuation, registering a low of 15 Mbps. Given that the network utilized a dedicated 30 Mbps backhaul, the performance at this distance is deemed to be backhaullimited, indicating that the wireless link was highly efficient and the bottleneck was external to the air interface. However, a dramatic and consistent drop in throughput occurs at extended distances, demonstrating the constraints imposed by poor wireless channel quality. At 6 m, the throughput is significantly reduced, ranging from 20 Mbps to 6.5 Mbps, and at 9 m, the performance falls sharply to critical levels, ranging from 10 Mbps to 2.8 Mbps. The network's inability to sustain high throughput at 9 m, despite the backhaul capacity, directly corroborates the extremely low SINR observed in Figure 9. This confirms that the severe reduction in SINR, which necessitates the use of inefficient low-order MCS, has replaced the backhaul as the primary performance bottleneck, leading to a diminished QoS for the end-user [33], [34].

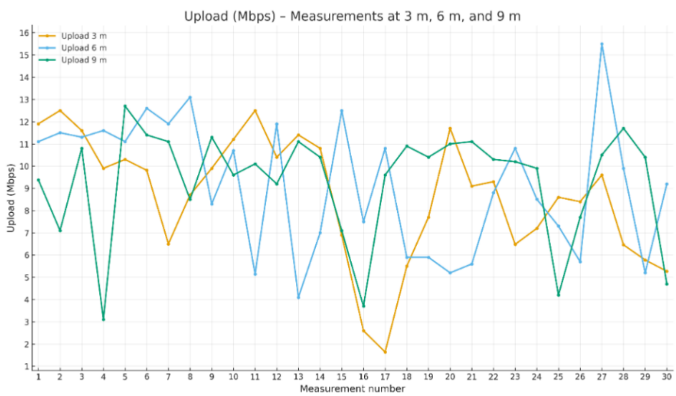

Figure 11. Measured upload values at distances of 3, 6, and 9 m

The performance trend observed in the downlink direction is mirrored in the Uplink Throughput performance. The results, presented in Figure 11, confirm the pervasive impact of channel degradation on bidirectional data rates. At 3 m, the uplink throughput achieved speeds up to a maximum of 12.5 Mbps, with the lowest recorded speed being 1.6 Mbps. This inherent volatility is common in uplink tests, which are often governed by the device's transmit power limitations and network scheduling efficiency. At 6 m, the throughput saw a reduction but remained relatively strong, recording a maximum of 15.5 Mbps and a minimum of 4.1 Mbps. Importantly, the peak throughput here surpassed that at 3 m, which can be attributed to dynamic factors such as the network scheduler prioritizing uplink resources at that specific distance or momentary channel conditions. However, the severe impact of poor channel quality is evident at 9 m, where the performance dropped significantly, recording a maximum of 12.7 Mbps and a minimum of 3 Mbps. Although the maximum uplink speed does not degrade as sharply as the downlink speed, this behavior is consistent with the eNodeB's control of uplink power control and uplink resource allocation, the increased frequency of low throughput values confirms that the underlying factors low

SINR and reliance on inefficient MCS severely restrict the device's ability to reliably transmit data packets, leading to a decreased QoE for uplink-heavy applications.

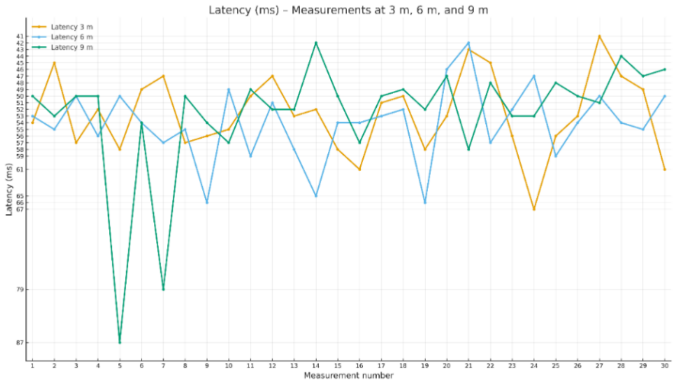

Figure 12. Measured latency values at distances of 3, 6, and 9 m

Figure 12 displays the final user-centric metric, latency. The measured latency shows a relatively stable performance across the near distances: the latency ranged from 41 to 67 ms at 3 m and from 42 to 66 ms at 6 m. These stable results suggest that the end-to-end delay is primarily dominated by base network processing and core network delay, rather than the physical path length itself. However, a noticeable increase in volatility occurs at 9 m, where the latency ranges from 42 ms to 87 ms. Compared with the 3-m measurement, this significant inflation in maximum latency directly reflects the severe channel degradation and low SINR observed in Figure 9. The observed increase in latency at extended distances is directly related to the degradation of SINR. Low SINR conditions result in higher Block Error Rates (BLER), which trigger frequent Hybrid Automatic Repeat Request (HARQ) retransmissions at the physical layer. These retransmissions significantly increase round-trip time and cause volatility in end-to-end latency, as observed at the 9 m measurement distance [35], [36]. This behavior confirms that radio channel quality, rather than core network processing, is the dominant contributor to latency degradation in low-power SDR-based LTE deployments.

4.2 RSRP Consistency and Data Accessibility on IoT Devices

Table 7. Measured RSRP values at distances of 3, 6, and 9 m with LTE IoT modem

Attempt	Distance (m)	RSRP
1	3	-92 dBm
2	6	-100 dBm
3	9	-105 dBm

Unlike multimedia-oriented services, flood monitoring systems primarily depend on lowbandwidth, periodic sensor telemetry, where transmission reliability and latency stability are more critical than achieving peak throughput [37], [38]. Therefore, the performance evaluation in this study prioritizes radio signal consistency and data accessibility on IoT devices rather than broadband service benchmarks. The IoT modem RSRP values, ranging between -92 dBm and - 105 dBm, consistently matched the average RSRP measured on the mobile phone, indicating stable experimental conditions and supporting the validity of the applied path-loss assumptions. However, a key limitation arises from the restricted access to essential radio-quality indicators on the IoT device, most notably SINR and RSRQ. This constraint precludes a comprehensive characterization of channel quality and link robustness, specifically concerning interference sensitivity and spectral efficiency estimation. To address this, future research will incorporate diagnostic-capable IoT terminals or interfaces that expose SINR/RSRQ metrics. Furthermore, the evaluation will be extended to include application-layer telemetry reliability metrics, ensuring the performance analysis more closely aligns with operational flood-monitoring requirements.

4.3 Telemetry Reliability and Timeliness (Flood Monitoring KPIs)

While broadband-centric metrics such as peak throughput and video-oriented Quality of Experience (QoE) are instrumental for benchmarking network capacity, they do not align with the functional requirements of periodic, low-rate flood telemetry. For critical applications like ultrasonic water-level monitoring, the performance envelope is instead defined by reliability and temporal consistency. Given that LTE systems mitigate degraded Signal-to-Interference-plusNoise Ratio (SINR) through robust Modulation and Coding Schemes (MCS) at the expense of increased retransmissions and tail latency, this study evaluates telemetry performance via two application-layer Key Performance Indicators (KPIs): Packet Delivery Ratio (PDR) and End-toEnd (E2E) Update Delay, characterized by median and 95th percentile ($^{P}95$) statistics.

The edge-based IoT devices generated telemetry updates for transmission to the central server through a private LTE infrastructure. These transmissions were conducted at controlled distances of 3 m, 6 m, and 9 m to evaluate performance across varying link conditions. To ensure rigorous end-to-end accounting, each data packet was encapsulated with a sequence number and an original generation timestamp. Upon successful delivery, the server-side logging mechanism recorded the precise time of arrival, allowing for accurate latency quantification. The specific parameters for this telemetry configuration are consolidated in Table 8.

Table 8. Telemetry test configuration

Parameter	Specification
Payload size	85 bytes
Transmission interval	1 s
Run duration	10 min
Repetitions	30
Acknowledged delivery	HTTPS

Over a 10 min run, each device generates 600 telemetry updates, so the flood-monitoring traffic remains sparse even before considering LTE scheduling granularity. For this reason, the dominant performance concern in the present use case is not peak throughput but whether updates continue to be delivered with high reliability and bounded delay as SINR degrades. This is why PDR and E2E update delay are adopted as the primary flood-monitoring KPIs, whereas broadband throughput results are retained only as secondary radio benchmark indicators. In addition, the effective conducted transmit power reported in Table 3 should be interpreted as a lower-bound estimate inferred from RSSI/FSPL reasoning, not as a direct calibrated conductedpower measurement.

Packet Delivery Ratio (PDR) quantifies telemetry reliability as the fraction of updates successfully received at the server/dashboard:

$$PDR = \frac{N_{delivered}}{N_{sent}} \tag{9}$$

Where:

a) N_{Sent} = total number of telemetry updates transmitted during a run.
b) $N_{delivered}$ = number of telemetry updates successfully received at the server/dashboard during the same run.

End-to-End Update Delay for each successfully delivered update is defined as:

$$D = t_{received} - t_{generated} \tag{10}$$

Where:

a) $t_{generated}$= telemetry generation timestamp at the edge device [ms].
b) $t_{received}$= reception timestamp at the server/dashboard [ms].
c) D = end-to-end update delay [ms].

Because early-warning systems are sensitive to latency outliers, delay is summarized using both the median and the 95th percentile P_{95}:

$$D_{50} = median(D),\ D_{95} = percentile_{95}(D) \tag{11}$$

These statistics capture typical timeliness (D_{50}) and tail latency behavior (D_{95}) that may increase under reduced SINR due to retransmissions and scheduling effects.

Figure 13 and Figure 14 provide a comprehensive evaluation of the system via PDR and endto-end delay metrics, respectively. While Figure 13 demonstrates the stability of periodic telemetry updates under changing radio conditions, Figure 14 emphasizes the impact of distance on tail latency using the 95th percentile (D_{95}). This increase in delay at the edge of the coverage area is a known consequence of HARQ processes and robust MCS selection required to maintain connectivity at lower SINR. Such metrics are far more representative for flood-monitoring applications than standard broadband throughput benchmarks, as they directly quantify the reliability and timeliness of mission-critical telemetry.

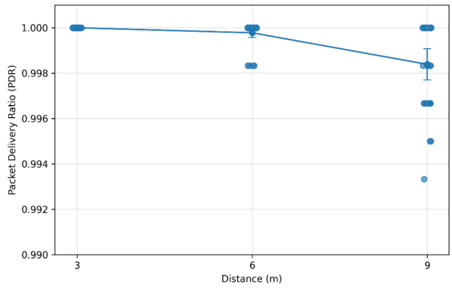

Figure 13. Telemetry Packet Delivery Ratio (PDR) versus distance (3 m, 6 m, 9 m)

Figure 13 indicates that telemetry delivery remains highly reliable across all evaluated distances. Over 30 runs per distance (18,000 updates per distance), the overall PDR was 1.00000 at 3 m (0 lost packets), 0.99978 at 6 m (4 lost packets), and 0.99839 at 9 m (29 lost packets). The mean PDR across runs remains close to unity, with narrow confidence intervals (95% CI: ±0.00021 at 6 m and ±0.00069 at 9 m), suggesting stable application-layer reliability despite distance-dependent radio degradation. Even at the farthest distance, the minimum per-run PDR observed was 0.99333, confirming that low-rate flood telemetry can be delivered consistently under the tested indoor conditions.

Figure 14 summarizes end-to-end telemetry update delay using both the median (D50) and the 95th percentile (D95) to capture typical and tail-latency behavior. As distance increases, the median delay rises from 109.88 ms at 3 m to 140.23 ms at 6 m and 181.00 ms at 9 m. The tail latency increases more noticeably: mean D95 grows from 174.08 ms (3 m) to 237.90 ms (6 m) and 342.20 ms (9 m). This widening gap between D_{50} and D_{95} at larger distances indicates that most telemetry updates still arrive within a relatively stable delay range, while a smaller fraction experiences longer delays consistent with retransmissions and conservative scheduling under reduced SINR. For early warning applications, the D95 trend is particularly important because increased tail latency can affect alarm timeliness even when overall delivery reliability remains high.

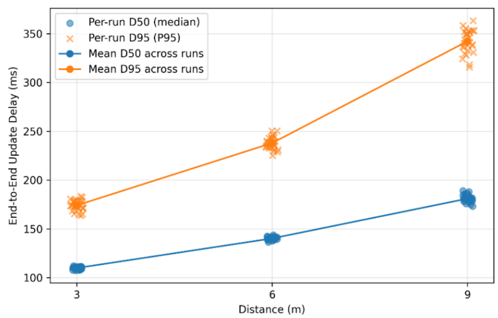

Figure 14. End-to-end sensor update delay versus distance (median and P_{95})

5. Conclusion

This study successfully characterized the performance and versatility of the developed private LTE network by analyzing signal quality and user experience metrics across varying radial distances. The results provide definitive evidence of the primary bottlenecks governing the capacity of the system. Signal analysis confirmed that RSRP, RSRQ, and SINR significantly degrade with distance, consistent with path loss and increased interference and multipath effects. The SINR drop from the "Excellent" category at 3 m to the "Fair" and "Poor" categories at 9 m established the compromised wireless channel as the primary limiting factor. This channel degradation directly impacted user performance, as evidenced by a drastic decrease in downlink throughput from 27 Mbps to 2.8 Mbps at 9 meters. Similarly, the dramatic increase in maximum latency to 87 ms was directly correlated with low signal-to-noise ratio, which induced higher Block Error Rates (BLER) and subsequent HARQ retransmissions. Despite these channel constraints, the proposed network demonstrated significant versatility. The assessment emphasized telemetry reliability and end-to-end latency to ensure the evaluation remained relevant to the intended flood-monitoring use case. Results presented in Figures 13 and 14 indicate that while high reliability is maintained across the tested range, tail latency (D_{95}) increases more significantly than the median delay as signal quality degrades. This behavior is consistent with LTE link adaptation and retransmission mechanisms under reduced SINR. While the prototype demonstrates technical feasibility for low-rate telemetry, the results underscore that practical field deployments require further hardware optimization. Future work aims to enhance the system for long-range outdoor operation through the integration of a dedicated PA and LNA to optimize the RF front-end. The deployment strategy will include higher-gain antennas and installation methods tailored for riverbank topography. Upcoming experimental campaigns will focus on characterizing LOS and NLOS propagation at distances of several hundred meters. Additionally, estimated power bounds will be replaced with calibrated conducted-power measurements. We also propose exploring bandwidth reduction as a strategy to increase noise margins, thereby prioritizing link robustness over peak throughput for missioncritical sensor updates.

Acknowledgement

I would like to express my deepest gratitude to Prof. Ir. Gunawan Wibisono, M.Sc., Ph.D., my principal supervisor, for his invaluable guidance, insightful feedback, and unwavering encouragement throughout the preparation of this study. I also extend my sincere appreciation to all faculty members and staff of the Department of Electrical Engineering, Faculty of Engineering, University of Indonesia, for their continuous support and provision of essential resources. This work was supported by the Faculty of Engineering, Universitas Indonesia, through the 2024 Reverse Engineering Grant for Entrepreneurship and Innovation, under the Dean's Decree Number 884 of 2024.

References

[1] Badan Pusat Statistik (BPS). *Jumlah Bencana Alam Menurut Provinsi dan Jenis Bencana Alam (kejadian)*. https://bit.ly/data-bps-jumlah-bencana-alam-menurut-provinsi-dan-jenis-bencana-alam-kejadian-2024. Accessed: Dec. 1, 2025. 2024.

[2] M. M. Myint and T. L. L. Thein. "Real-time Flood Monitoring System using Internet of Things in Urban". In: *IEEE Conference on Computer Applications (ICCA)*. Mar. 2025, pp. 1–4. DOI: 10.1109/ICCA65395.2025.11011054.

[3] M. Zafar-uz-Zaman. "A Review on the Evolution of Cellular Technologies". In: *16th International Bhurban Conference on Applied Sciences & Technology (IBCAST)*. 2019. DOI: 10.1109/IBCAST.2019.8667173.

[4] V. V. Garbhapu and S. Gopalan. "LTE-M for IoT Healthcare - Regression or Adaptation?" In: *IEEE AFRICON*. 2023. DOI: 10.1109/AFRICON55910.2023.10293713.

[5] F. Ramon et al. "LTE: The Technology Driver for Future Public Safety Communications". In: *IEEE Communications Magazine* 51 (Oct. 2013). DOI: 10.1109/MCOM.2013.6619579.

[6] H. Dui, H. Zhang, and S. Wu. "A IoT-Based Novel Methodology to Optimize Multidimensional Flood Resilience of Drainage Systems for Sponge City". In: *Sustainable Cities and Society* 130 (July 2025). DOI: 10.1016/j.scs.2025.106523.

[7] M. I. Zakaria, W. A. Jabbar, and N. Sulaiman. "Development of a Smart Sensing Unit for LoRaWAN-Based IoT Flood Monitoring and Warning System in Catchment Areas". In: *Internet of Things and Cyber-Physical Systems* 3 (2023), pp. 249–261. DOI: 10.1016/j.iotcps.2023.04.005.

[8] C. Prakash, A. Barthwal, and D. Acharya. "FLOODWALL: A Real-Time Flash Flood Monitoring and Forecasting System Using IoT". In: *IEEE Sensors Journal* 23.1 (2023), pp. 787–799. DOI: 10.1109/JSEN.2022.3223671.

[9] OECD. *Enhancing the Resilience of Communication Networks*. Tech. rep. Paris, May 2025. DOI: 10.1787/d6920477-en.

[10] S. Majumdar, L. A. Szolga, and S. Kirkley. "IoT-Enabled Autonomous Vehicles for Wildfire Relief: A System of Systems Approach". In: *iEECON 2025*. 2025. DOI: 10.1109/iEECON64081.2025.10987618.

[11] F. Neto, J. Granjal, and V. Pereira. "A Survey on Security Approaches on PPDR Systems Toward 5G and Beyond". In: *IEEE Access* 10 (2022), pp. 117118–117140. DOI: 10.1109/ACCESS.2022.3217223.

[12] I. Makino et al. "Throughput and Delay Performance Measurements in Multi-Floor Building Employing Private LTE". In: *IEEE Access* 10 (2022), pp. 24288–24301. DOI: 10.1109/ACCESS.2022.3153702.

[13] K. Gomez and L. Goratti. "Enabling Disaster-Resilient 4G Mobile Communication Networks". In: *IEEE Communications Magazine* 52 (Dec. 2014). DOI: 10.1109/MCOM.2014.6979954.

[14] N. et al. Mishra. "Scaling Out srsRAN Through Interfacing Wirelessly srsENB with srsEPC". In: *IEEE INFOCOM Workshops*. 2023. DOI: 10.1109/INFOCOMWKSHPS57453.2023.10225836.

[15] I. Shostko et al. "Introduction of Private LTE Networks to Provide Specific Communication Tasks". In: *PIC S&T*. 2021, pp. 583–586. DOI: 10.1109/PICST54195.2021.9772142.

[16] O. Sahin, V. Sathya, and M. Yavuz. "Private Networks: Evolution, Ecosystem, Use Cases, Architecture, Spectrum, and Deployment Challenges". In: *Computer Communications* 242 (2025). DOI: 10.1016/j.comcom.2025.108295.

[17] B. et al. Chen. "Construction and Application of a Private 5G Standalone Medical Network". In: *Journal of Medical Internet Research* 26.1 (2024). DOI: 10.2196/52404.

[18] D. M. Molla et al. "Software Defined Radio Platforms for Wireless Technologies". In: *IEEE Access* 10 (2022), pp. 26203–26229. DOI: 10.1109/ACCESS.2022.3154364.

[19] D. M. Brennan and V. Marojevic. "UHD-DPDK Performance Analysis for Advanced Software Radio Communications". In: *DCOSS*. 2022, pp. 420–425. DOI: 10.1109/DCOSS54816.2022.00076.

[20] S. B. S. Hanbali. "Low-Cost Software-Defined Radio for Electrical Engineering Education". In: *IEEE Potentials* 42.5 (2023), pp. 13–19. DOI: 10.1109/MPOT.2022.3223788.

[21] D. Erdosy, T. Bodolai, and I. Bodnar. "Precompliance Testing Using Software Defined Radio". In: *23rd International Carpathian Control Conference (ICCC)*. 2022, pp. 404–407. DOI: 10.1109/ICCC54292.2022.9805858.

[22] M. S. Gawade and R. D. Joshi. "GNU Radio and USRP B210 Based Software Defined Radio for OFDM Data Transmission". In: *IEEE International Conference on Mobile Networks and Wireless Communications (ICMNWC)*. 2021. DOI: 10.1109/ICMNWC52512.2021.9688506.

[23] N. Apostolakis, M. Gramaglia, and P. Serrano. "Design and Validation of an Open Source Cloud Native Mobile Network". In: *IEEE Communications Magazine* 60 (2022). DOI: 10.1109/MCOM.003.2200195.

[24] S. Shen and H. Li. "A Platform Based on srsRAN for Security Research in LTE Network". In: *4th Information Communication Technologies Conference (ICTC)*. 2023, pp. 40–43. DOI: 10.1109/ICTC57116.2023.10154848.

[25] M. Motaung et al. "Comparative Analysis of 5G SDR-Based Open-Source Software Platforms: OpenAirInterface and srsRAN". In: *IEEE 3rd Wireless Africa Conference (WAC)*. Feb. 2025, pp. 1–7. DOI: 10.1109/WAC63911.2025.10992595.

[26] A. S. Yogapratama, U. K. Usman, and T. A. Wibowo. "Analysis on 900 MHz and 1800 MHz LTE Network Planning in Rural Area". In: *3rd International Conference on Information and Communication Technology (ICoICT)*. Nusa Dua, Bali, Indonesia, 2015. DOI: 10.1109/ICoICT.2015.7231410.

[27] A. Ribeiro, N. Medeiros, and N. Cota. "Comparison of GSM, WCDMA and LTE Performance on 900 MHz Band". In: *Procedia Technology* 17 (2014), pp. 674–682. DOI: 10.1016/j.protcy.2014.10.208.

[28] F. Afroz et al. "SINR, RSRP, RSSI and RSRQ Measurements in Long Term Evolution Networks". In: *International Journal of Wireless & Mobile Networks* 7.4 (Aug. 2015), pp. 113–123. DOI: 10.5121/ijwmn.2015.7409.

[29] A. Elnashar and M. A. El-Saidny. "Looking at LTE in Practice: A Performance Analysis of the LTE System Based on Field Test Results". In: *IEEE Vehicular Technology Magazine* 8.3 (2013), pp. 81–92. DOI: 10.1109/MVT.2013.2268334.

[30] S. Avallone et al. "Experimental Characterization of LTE Adaptive". In: *IEEE International Workshop on Measurement and Networking (M&N)*. 2017. DOI: 10.1109/IWMN.2017.8078401.

[31] S. Mammen. *Making Sense of Signal Strength/Signal Quality Readings for Cellular Modems*. https://www.nealsystems.com/images/pdf/Industrial-Networking-Solutions-Tips-and-Tricks.pdf. Accessed: Dec. 15, 2025.

[32] G. M. Putra et al. "4G LTE Experience: Reference Signal Received Power, Noise Ratio and Quality". In: *East Indonesia Conference on Computer and Information Technology (EIConCIT)*. Apr. 2021, pp. 139–144. DOI: 10.1109/EIConCIT50028.2021.9431853.

[33] S. Shrestha et al. "Quantification of Interference Constraint for Small Cells in Low SINR Regime With Steepest Ascent Method". In: *IEEE Access* 13 (2025), pp. 2328–2339. DOI: 10.1109/ACCESS.2024.3524671.

[34] X. Xu, M. Ni, and R. Mathar. "Improving QoS by Predictive Channel Quality Feedback for LTE". In: *International Conference on Software, Telecommunications and Computer Networks (SoftCOM)*. 2013. DOI: 10.1109/SoftCOM.2013.6671880.

[35] I. Parvez et al. "A Survey on Low Latency Towards 5G: RAN, Core Network and Caching Solutions". In: *IEEE Communications Surveys & Tutorials* 20.4 (Oct. 2018), pp. 3098–3130. DOI: 10.1109/COMST.2018.2841349.

[36] G. Gómez et al. "Towards a QoE-Driven Resource Control in LTE and LTE-A Networks". In: *Journal of Computer Networks and Communications* 2013 (2013), p. 505910. DOI: 10.1155/2013/505910.

[37] J. Aranda et al. "A Framework for Multimodal Wireless Sensor Networks". In: *Ad Hoc Networks* 106 (2020), p. 102201. DOI: 10.1016/j.adhoc.2020.102201.

[38] U. K. Thakur. "QoS Aware Cloud Based Routing Protocol for Security Improvement of Hybrid Wireless Network". In: *Machine Learning Research* 4.1 (2019), p. 21. DOI: 10.11648/j.mlr.20190401.14.